Aerosol radiative effects in photosynthetically active radiation and total irradiance at a Mediterranean site from an 11-year database

Lozano, Ismael López

2021

Lozano , I L , Sánchez-Hernández , G , Guerrero-Rascado , J L , Alados , I & Foyo-Moreno , I 2021 , ' Aerosol radiative effects in photosynthetically active radiation and total irradiance at a Mediterranean site from an 11-year database ' , Atmospheric Research , vol. 255 . https://doi.org/10.1016/j.atmosre

http://hdl.handle.net/10138/355357
https://doi.org/10.1016/j.atmosres.2021.105538

Aerosol radiative effects in photosynthetically active radiation and total irradiance at a Mediterranean site from an 11-year database

Ismael L. Lozano[1,2], Guadalupe Sánchez-Hernández[1,2], Juan Luis Guerrero-Rascado[1,2], Inmaculada Alados[1,3], Inmaculada Foyo-Moreno[1,2]

[1]Andalusian Institute for Earth System Research, Granada, 18006, Spain

[2]Department of Applied Physics, University of Granada, Granada, 18071, Spain

[3]Applied Physics II Department, University of Málaga, Málaga, 29071, Spain

Corresponding author: ifoyo@ugr.es

https://doi.org/10.1016/j.atmosres.2021.105538

Abstract

This study addresses the analysis of the aerosol radiative forcing (ARF) and aerosol forcing efficiency (AFE) at surface in the Photosynthetically Active and Total radiation ranges in a Southwest Mediterranean site. A thorough analysis of a long-term database (2008-2018) has been performed, bringing very valuable results about both, the absolute values and trends in ARF and AFE for both spectral intervals. The largest monthly mean for aerosol optical depth at 500 nm (AOD_{500}) is found in summer (0.16 at July and August) meanwhile the lowest value is in winter (0.08 at November and December), with an interannual range varying from 0.11 ± 0.03 (in 2018) to 0.17 ± 0.03 (in 2014). The AFE variation range has been estimated between -12 and -198 $Wm^{-2}\tau^{-1}$ for PAR and between -9 and -450 $Wm^{-2}\tau^{-1}$ for Total irradiance. ARF varies between -1 Wm^{-2} and -23 Wm^{-2} in the PAR range, taking values from -1 to -40 Wm^{-2} in the Total one. This result points out the relevance of the aerosol effects on the PAR range, which can involve up to a 50% of the Total ARF. Moreover, a notable dependence of ARF and AFE on the solar position has been detected, increasing their absolute values at solar zenith angle from 0^{o} to 45^{o}-60^{o} and decreasing to zero for lower solar positions. Additionally, this analysis has revealed the existence of a significant downward trend in AFE values for PAR, with a slope of 2.7 $Wm^{-2}\tau^{-1}year^{-1}$. Although the slope is positive, taking into account that the AFE values are negative, the slope value implies that the aerosol cooling radiative effect of aerosols is decreasing. However, no trends have been detected neither in AFE nor ARF values in the Total solar range. These results evidence the long-term aerosol effects over the different spectral intervals and emphasize the need for detailed analysis of the aerosol radiative effects on fundamental spectral intervals such as the PAR range.

Keywords: Aerosols; Photosynthetically active radiation; Radiative forcing.

1.- INTRODUCTION

Photosynthetically Active Radiation (PAR) is commonly defined as the electromagnetic radiation in the waveband between 400 and 700 nm (McCree, 1972). This spectral interval, which contains the maximum of the solar radiation spectrum, plays a fundamental role in vegetation productivity and agricultural research (Caya et al., 2018; McCree, 1981). PAR is the driver of the photosynthesis process and the biochemical reactions involved in it (Wu et al., 2019) and, therefore, the beginning of the plant growth. Moreover, PAR is a key factor controlling ecological processes such as the terrestrial carbon and hydrological cycles (Jonard et al., 2020; Potter et al., 2007, 2008).

Along its path throughout the atmosphere, solar radiation, and particularly PAR, is attenuated by scattering and absorbing processes, being atmospheric aerosols, the main

https://doi.org/10.1016/j.atmosres.2021.105538

factor determining the amount and distribution of solar radiation reaching the Earth's surface in absence of clouds. Aerosol particles affect the Earth's radiation budget both directly, by scattering and absorption, and indirectly, modifying cloud properties (e. g. Eswaran et al., 2019; Farahat et al., 2016; Satheesh & Krishna Moorthy, 2005). Aerosol attenuation presents an important spectral dependence. Thus, while spectral aerosol absorption decreases with wavelength, aerosol scattering efficiency strongly depends on the aerosol composition, increasing with wavelength for mineral dust and decreasing in case of urban pollution (Bergstrom et al., 2007). Due to this spectral dependence of the attenuation processes, aerosol effects over shorter wavelengths, such as the PAR interval, take a special relevance (Xu et al., 2003).

In order to quantify the radiative balance variations due to changes in atmospheric aerosols, the concepts of aerosol radiative forcing (ARF) and aerosol forcing efficiency (AFE) are widely employed. ARF is defined as the change in the net radiation due to variations in the atmospheric aerosol properties with respect to an aerosol-free atmosphere. ARF highly depends on the aerosol size distribution and composition (e.g. Foyo-Moreno et al., 2014). Thus, while mineral dust particles show negative ARF values associated to a strong cooling, the anthropogenic aerosols exhibit a complex behavior, with positive and negative ARF values depending on many factors such as greenhouse gases and surface changes (e.g. Andreae et al., 2005; Charlson et al., 1991; Esteve et al., 2012; Gopal et al., 2014; Hansen et al., 2011; Satheesh & Krishna Moorthy, 2005; Zhuang et al., 2013). On the other hand, AFE is defined as the rate at which the atmosphere is forced per unit of aerosol optical depth, allowing for a more detailed assessment of the radiative forcing considering the aerosol type.

https://doi.org/10.1016/j.atmosres.2021.105538

Several studies have analyzed the impact of different aerosol types, and particularly their ARF, on total solar radiation (280-3000 nm) worldwide (e.g. Sicard et al., 2016; Sorribas et al., 2019; Zhang et al., 2018). However, aerosol radiative effects and its relationship to climate change remain inaccurate (IPCC 2013; Stocker et al., 2013). This uncertainty is larger in the PAR range because of the scarcity of related studies (Lyamani et al., 2006a; Mateos et al., 2014; Zhu et al., 2015). In fact, a worldwide routine network for the measurement of PAR is not yet established and PAR is often calculated as a constant ratio of the Total irradiance (Alados et al., 1996; Ge et al., 2011). Thus, one of the main drawbacks for this type of analysis is the lack of simultaneous and reliable measurements of PAR and aerosol properties. This limitation is stronger when the analysis is focused on trends in long-term databases and on the Mediterranean region (Di Biagio et al., 2009).

Recently, Obregón et al. (2020) studied the spatial and temporal AOD variations and the effects on solar radiation at the surface in the Mediterranean basin during a long period (2000–2018). Previously, they quantified ARF and AFE at Évora (Portugal, Southwestern Iberian Peninsula) during thirteen years (Obregón et al., 2017). In this Mediterranean region, temperature is increasing faster than the world average during the last decades (Lionello et al., 2014), and climate projections predict an increase of extreme climatic events, such as heat waves and droughts (Garcia-Herrera et al., 2014; Lionello et al., 2014). Besides, the Mediterranean region is subject to high aerosol loads, especially during spring and summer (Nabat et al., 2015), leading this region as a benchmark for climatic effect studies.

https://doi.org/10.1016/j.atmosres.2021.105538

In this context, this aims to assess the aerosol radiative effects at surface on PAR for an urban middle-latitude site (Granada) in the Mediterranean basin for the decade 2008-2018. Local aerosols sources are traffic, local mineral dust during the dry season, and anthropogenic aerosols in winter from fuel oil combustion for domestic heating (Titos et al., 2012, 2017). At the same time, this site is also frequently influenced by emissions of several allochthonous aerosols sources such as continental aerosols from Europe and mineral dust from Africa (Fernández et al., 2019; Guerrero-Rascado et al., 2008, 2009; Lyamani et al., 2006a, 2006b, 2010), transported smoke from North America, North Africa and Europe (Alados-Arboledas et al., 2011; Baars et al., 2019; Ortiz-Amezcua et al., 2014; 2017; Titos et al., 2017), extraordinarily, aerosols events from volcanic plumes (Navas-Guzmán et al., 2013; Sicard et al., 2012), and oceanic aerosols from Arctic and Atlantic oceans or maritime aerosols from the Mediterranean sea (Cariñanos et al., 2021; Pérez-Ramírez et al., 2016). Due to this variety in aerosol sources and types, aerosols over Granada are complex and variable making this an attractive region for the analysis of the aerosol radiative effects.

To this aim, AFE and ARF values for the PAR and Total ranges for cloud-free situations have been estimated, and analyzed in detail for different years and solar positions. Additionally, potential AFE and ARF trends at both spectral ranges, PAR and Total, have been assessed and compared.

2.- EXPERIMENTAL SITE AND DATASET

https://doi.org/10.1016/j.atmosres.2021.105538

Measurements used in this study have been collected at the radiometric station installed on the roof of the IISTA-CEAMA building at Granada (37.16 ºN, 3.61 ºW, 680 m.a.s.l.), an urban site located in the Southeast of Spain in the West Mediterranean region. This radiometric station is managed by the Atmospheric Physic Research Group (GFAT) at the University of Granada and is part of the observatory AGORA (Andalusian Global ObservatoRy of the Atmosphere) in the framework of ACTRIS (Aerosol, Clouds and Trace Gases Research Infrastructure). The period analyzed encompasses the decade 2008-2018. Granada presents large seasonal temperature differences, characterized by cool winters and hot summers, with mean daily maximum temperature at surface of (14.6 ± 2.4) ºC in winter and (32 ± 3) ºC for 1981-2010 period (AEMET, Spanish Meteorology Statal Agency).

In this study, one-minute measurements of Photosynthetically Active Radiation (PAR) were measured with a SKP 215 PAR Quantum Sensor (#28715) manufactured by Skye Instruments. This instrument measures the solar radiation in the range of 400-700 nm using a blue enhanced planar diffused silicon detector with a sensitivity of 0.015 $\mu A/\mu mol\ m^{-2}s^{-1}$. The quantum sensor has a maximum relative error <5%. Simultaneous one-minute measurements of total solar irradiance were recorded with a radiometer CM11 (#861452) manufactured by Kipp&Zonen. This instrument measures broadband solar irradiance in the range of 280-2800 nm and complies with International Organization for Standardization (ISO) 9060 criteria for an ISO secondary standard pyranometer. Both measurements were recorded in a CR10X data logger manufactured by Campbell Scientific.

https://doi.org/10.1016/j.atmosres.2021.105538

Additionally, Aerosol Optical Depth (AOD) values, measured every 15 minutes by a CIMEL Sun/sky photometer (CE-318-4) were used in this study. This instrument, which is integrated in the AERONET network (Holben et al., 1998), measures direct solar irradiance with a 1.2° full field of view at 340, 380, 440, 500, 675, 870, 940 and 1020 nm as well as sky radiances in the almucantar and principal plane geometries at 440, 675, 870 and 1020 nm. All radiance measurements are processed following the AERONET protocol as described by Holben et al. (1998), obtaining columnar aerosol properties at different quality levels (1.0, 1.5, 2.0). Version 3 of AOD at level 2.0 (Giles et al., 2019), the highest quality AERONET data, was used in this study, except for 2014 for which only version 2 at 2.0 level AOD was available. AOD data has a total uncertainty of 0.01 for wavelengths ≥ 440 nm and 0.02 for shorter wavelengths (Holben et al., 1998). Sun-photometer also provided the surface albedo measurements used in this study at 440, 675, 870 and 1020 nm with a total uncertainty of 0.02 (Foyo-Moreno et al., 2014). Both, CIMEL photometer and radiometers involved in this study have been intercompared respect to reference instruments several times along the 11-year period analyzed, with their last intercomparison dated on May 2020 for the CIMEL photometer, May 2019 for the CM11 pyranometer and August 2020 for the PAR sensor. CIMEL were calibrated following AERONET protocols (Holben et al., 1998) at the RIMA calibration facilities at Valladolid, Spain, while the radiometers have been intercompared with a Kipp&Zonen CMP21 and a LICOR-190SA, respectively, following WMO procedure for intercomparison (WMO, 2008). Particularly, the calibration factors applied in this study showed a change of 0.15 mV/Wm^{-2}, in CM11 pyranometer, and 0.4 mV/Wm^{-2}, in PAR sensor, for the entire period 2008-2018. This involves an annual average change of 0.013 $mV/Wm^{-2}\ year^{-1}$ and 0.027 $mV/Wm^{-2}\ year^{-1}$ for Total and PAR irradiance sensor, respectively. Both values are

https://doi.org/10.1016/j.atmosres.2021.105538

notably below the maximum change per year (long-term stability) detailed by the corresponding manufacturer, 0.5% for the CM11 and 2% for SKP 215 PAR Quantum Sensor, ensuring the calibration factor stability required for a trend analysis.

3.- METHODOLOGY

3.1 Data analysis and selection of cloud-free scenarios

To perform the analysis of the aerosol radiative effects, a database of simultaneous measurements of PAR, Total irradiance and AOD has been built for the period 2008-2018. This vast database ensures a large variety of seasonal processes, solar geometries and meteorological conditions and guarantees the representativeness of the dataset for the analysis proposed here.

A deep quality control has been applied to this final dataset in order to detect and eliminate potential erroneous measurements. First, only those measurements recorded for solar zenith angles smaller than 80º have been selected to avoid solar radiation data affected by a cosine response error, the maximum difference from the ideal response for PAR Quantum Sensor was approximately 7% at a zenith angle of 80º (Akitsu et al., 2017). Additionally, those cases in which total global irradiance reached higher values than extraterrestrial total irradiance (k_t > 1) or diffuse irradiance higher than global irradiance (k_d > 1) were removed. Outliers were detected by visual inspection and consequently removed. Possible troubles associated with power supply and temperature of the acquisition system were also checked.

https://doi.org/10.1016/j.atmosres.2021.105538

Additionally, a thorough analysis of the AOD values along the period of study has been performed. Thus, data has been monthly grouped along the entire period in order to analyze seasonal evolution and a detailed statistical has been computed including arithmetic mean (Ave), standard deviation (SD), median (Md), minimum (Min), maximum (Max), percentiles 5^{th}, 25^{th}, 75^{th} and 95^{th} (P5, P25, P75 and P95, respectively), skewness (Ske), kurtosis (Kur) and the variation coefficient (VC) defined as the ratio between SD and the arithmetic mean.

In order to only account for aerosol effects, cloud-free situations have been selected applying the criterion proposed by Alados-Arboledas et al. (2000). This criterion detects as cloud-free situations those in which:

$$k_t > 0.53 + 0.31 \cos SZA - 0.15 \cos^2 SZA \qquad (1)$$

where k_t is the clearness index, defined as the ratio between the total irradiance ground-measured and the extraterrestrial total irradiance ($G_{ext} = E_o I_{sc} \cos SZA$), both on a horizontal plane, where SZA is the solar zenith angle, E_o is the eccentricity correction factor and the value used of the Solar Constant (I_{sc}) is 1367 Wm^{-2} (Iqbal, 1983). The variability of the Solar Constant on the 11-year solar cycle has not been considered in this study. This empirical criterion, based on coefficients derived from a fitting to a polynomial function has been explicitly developed for Granada. This criterion only requires global irradiance measurements, commonly available at most radiometric stations.

3.2 AFE and ARF estimation

https://doi.org/10.1016/j.atmosres.2021.105538

The ARF is defined as the difference between the measured net irradiance (F_{net}) and the same magnitude for an aerosol-free atmosphere ($F_{net,a}$):

$$ARF = F_{net} - F_{net,a} \quad (2)$$

where F_{net} is the difference between the downward and the upward irradiances at the Earth's surface. Net irradiances under the presence/absence of aerosols can be written, respectively, as:

$$F_{net} = (1 - A)I \quad (3)$$

$$F_{net,a} = (1 - A)I_a \quad (4)$$

where I is the experimental irradiance, I_a is the estimated irradiance under absence of aerosols, and A is the surface albedo.

The aerosol forcing efficiency (AFE) is defined as the change in ARF per unit increase in AOD for a certain wavelength (Bush and Valero, 2003):

$$AFE = \frac{dARF}{dAOD} \quad (5)$$

Thus, AFE at surface can be computed from the slope of the linear regression between ARF and AOD at fixed SZA (Antón et al., 2011; Díaz et al., 2007; García et al., 2006).

Different methodologies to estimate ARF have been proposed in literature. An extended method involves the use of radiative transfer models to estimate the net irradiance fluxes (Eswaran et al., 2019; Mateos et al., 2014; Sivan & Manoj, 2019). However, this procedure involves relevant assumptions such as the atmospheric composition and the aerosol layer description, which could lead to important errors. In this study, the so-

https://doi.org/10.1016/j.atmosres.2021.105538

called direct method proposed by Satheesh and Ramanathan (2000) has been used. Once cloud-free situations have been selected from the database, AFE is derived as the slope of the linear fit between the experimental F_{net} values and AOD at fixed SZA:

$$AFE = \frac{dF_{net}}{dAOD} \tag{6}$$

Then, ARF at surface is obtained as a result of multiplying AFE by the annual AOD average at the corresponding solar position (Di Biagio et al., 2010; Foyo-Moreno et al., 2014). The advantage of this method is that AFE is directly computed from the experimental data without further assumptions on the radiative fluxes under aerosol-free conditions. This method shows an important dependence on the solar zenith angle and, therefore, its application and analysis is limited to specific solar zenith intervals.

Particularly, AOD values at 500 nm have been used to analyze the aerosol effects on the PAR for roughly being the central wavelength in this spectral range. On the other hand, AOD at 675 nm has been chosen to estimate AFE and ARF for the Total irradiance considering that the central wavelength of the solar spectrum is roughly 680 nm (Di Biagio et al., 2010). This decision is also supported by previous works (e.g. Foyo-Moreno et al., 2014; Li et al., 2020; Romano et al., 2016).

Additionally, five categories of solar zenith angles to compute both AFE and ARF, namely 15°, 30°, 45°, 60° and 75° (±1°), have been considered, in order to cover the majority of solar positions. Moreover, surface albedo provided by AERONET at 675 nm for our station has been used. Annual average surface albedo was estimated and employed in the calculation of the ARF, being 0.14 the annual average for all years, except for 2009

https://doi.org/10.1016/j.atmosres.2021.105538

and 2013 for which a value of 0.15 was found. The overall error in next flux increases by less than 0.3% due to the uncertainty in surface albedo (Di Biagio et al., 2010).

3.3 Trend analysis

Finally, the non-parametric Mann-Kendall test (Mann, 1945) has been applied to detect time series trends for AOD, ARF and AFE with statistical significance. In addition, the Sen estimation of the trend slope has been performed, which complements the Mann-Kendall test (Sen, 1968). The use of the Sen method is appropriate for evaluating trends in time series as it is not affected by outliers and gaps, making it a common method in literature (e.g. Buffoni et al., 1999; Da Silva et al., 2010; Dadashi-Roudbari and Ahmadi, 2020; Kodera et al., 2008; Kuo et al., 2020; Olmo & Alados-Arboledas, 1995; Zou et al., 2016). To perform these calculations the kbtau.m software developed by Jeff Burkey (*Mann-Kendall Tau-b with Sen's Method (Enhanced)*, 2020) was used.

4.- RESULTS AND DISCUSSION

4.1 AOD characterization

First, to have a brief global view, a general characterization of the whole databases including all variables analysed has been included in Figure 1, showing the monthly averages for every year. The two data series for the solar irradiance measurements display the same typical annual cycle with summer maximum (for example, (730 ± 60) Wm^{-2} for Total and (340 ± 30) Wm^{-2} for PAR in July 2016) and winter minimum, driven by the annual course of the solar zenith angle, with interannual variability.

https://doi.org/10.1016/j.atmosres.2021.105538

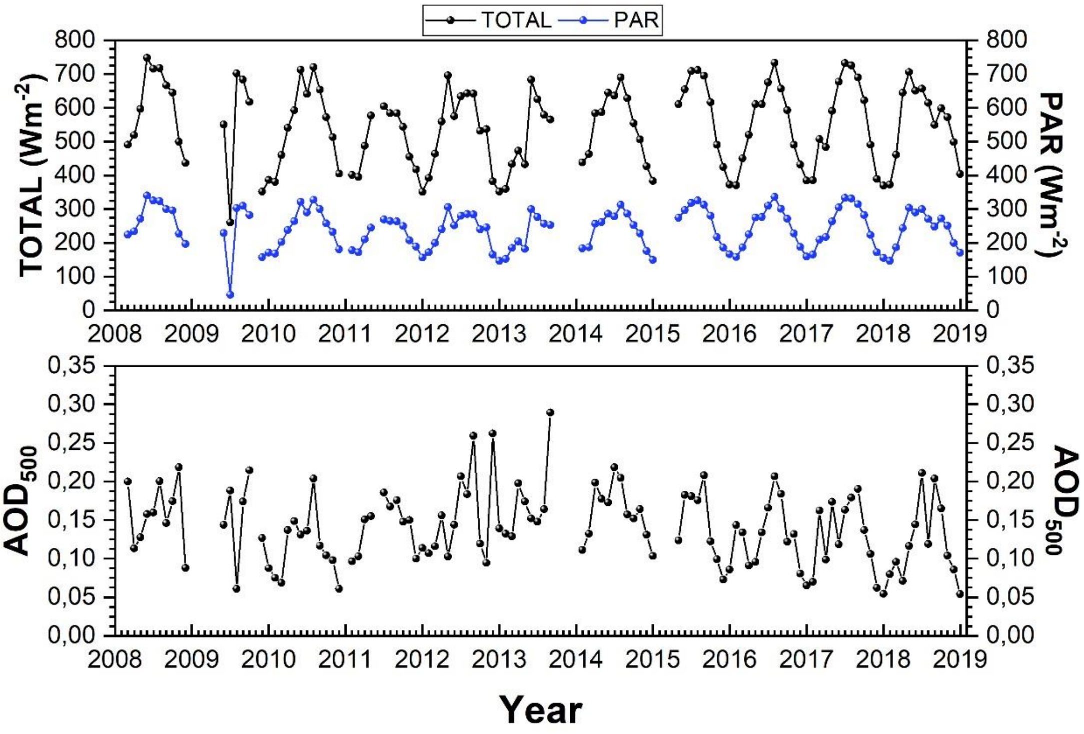

Figure 1. Time series of monthly mean PAR (black line), Total (blue line) and AOD at λ= 500nm (AOD_{500}), for 2008-2018 years.

Focusing on AOD, for the sake of clarity, the analysis of AOD is presented here based on 500 nm (Table 1 and Figure 2). The largest monthly mean AOD_{500} is found in summer (0.16 at July and August) meanwhile the lowest values are in winter (0.08 at November and December. The maximum/minimum values occur, respectively, in summertime due to the higher frequency Saharan dust outbreaks (Salvador et al., 2014), and in wintertime due to the low probability of these events (Gkikas et al., 2013, 2018; Querol et al., 2009) over the Mediterranean region. This behaviour agrees with previous studies. Mateos et al. (2014) reported a minimum and maximum AOD_{440} in November and July, respectively, at the same location during the period 2004-2012. Antón et al. (2011) found minimum AOD_{380}(0.14 ± 0.05) and AOD_{400} (0.12 ± 0.05) in November and

https://doi.org/10.1016/j.atmosres.2021.105538

December, respectively, coinciding in time with our minimum AODs, but differing with respect to maximum values found in May (0.26 ± 0.12 for AOD_{380} and 0.24 ± 0.12 for AOD_{440}). These differences might be caused by the short period used (2006-2008), probably limiting its representativeness. In a later study, Mateos et al. (2015) studied the aerosol load over the Iberian Peninsula in five geographical sectors and they found values for AOD_{440} varying between 0.15 and 0.20. This annual cycle is also found by Bennouna et al. (2016) for long measurement records (2003-2014) obtained at two sites of Spain located in the North Central region, with values for AOD_{440} of 0.16 ± 0.09 in June and 0.08 ± 0.06 in December. Segura et al. (2017) found a mean value of 0.15 ± 0.11 for AOD_{550} with the same seasonal pattern for a site located Mediterranean coastal area in Spain during the period 2007-2016. Sicard at al. (2016) also found for AOD_{440} a clear annual cycle (maxima of 0.22 at Ersa and 0.27 at Palma observed in July) for a 5-year period for different locations in the Western Mediterranean Basin.

Table 1. Monthly statistics of AOD_{500} for the period 2008-2018 based on daily values: Number of datapoints (N), Average (Ave), Standard deviation (SD), Median (Md), Percentiles (P5, P25, P75, P95), Skewness (Ske), Kurtosis (Kur) and coefficient of variation (CV).

Month	N	Ave	Md	P5	P25	P75	P95	Ske	kur	CV(%)
January	3603	0.09±0.06	0.08	0.03	0.06	0.11	0.20	2.19	10.92	63
February	3840	0.11±0.06	0.10	0.04	0.07	0.14	0.21	1.73	9.51	54
March	4641	0.13±0.07	0.11	0.05	0.08	0.16	0.26	1.89	9.20	54
April	5158	0.13±0.07	0.12	0.05	0.08	0.16	0.25	2.20	11.36	54
May	6986	0.13±0.07	0.13	0.06	0.09	0.17	0.25	2.17	12.12	51
June	10344	0.15±0.09	0.14	0.05	0.09	0.21	0.34	1.50	5.65	60
July	13132	0.16±0.09	0.15	0.05	0.09	0.22	0.34	1.20	4.61	58
August	10763	0.16±0.09	0.15	0.05	0.10	0.22	0.34	1.39	6.73	58
September	8447	0.13±0.07	0.12	0.05	0.08	0.17	0.26	1.35	5.43	55
October	6529	0.11±0.06	0.10	0.04	0.07	0.15	0.24	1.51	7.57	56
November	4771	0.08±0.05	0.07	0.03	0.05	0.10	0.16	2.90	20.63	63
December	3436	0.08±0.04	0.07	0.03	0.05	0.10	0.16	1.68	7.67	53

https://doi.org/10.1016/j.atmosres.2021.105538

The analysis of P5 and P95 is similar to the trend of the average values. The median AOD values are smaller than the mean, what is a common feature over the Iberian regions (Mateos et al., 2015). The absolute difference between the median and third quartile is also larger than the absolute difference between the median and the first quartile except at two months, namely April and May. This last result is also in accordance with those found by Mateos et al. (2015). The kurtosis and asymmetry data for AOD show that the distribution for all months is leptokurtic and positive asymmetric, obtaining the highest asymmetry values for November, while the lowest values are found in July.

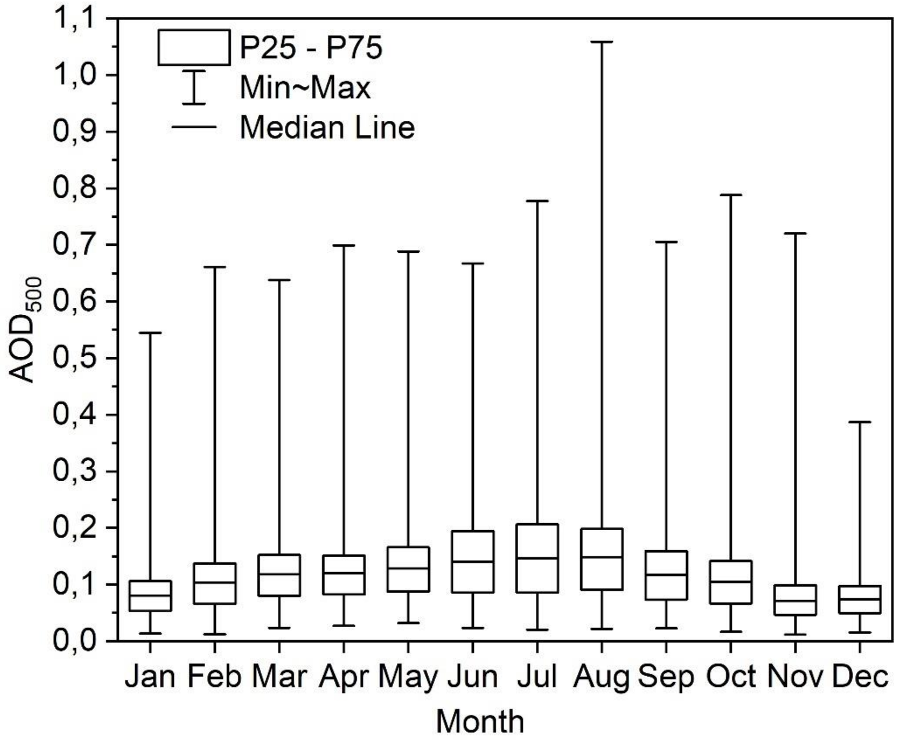

Figure 2. Monthly statistics of AOD_{500} for the period 2008-2018. Bars correspond to the minimum and maximum values, the box limits are the P25 and P75 percentiles and the midline is the median.

https://doi.org/10.1016/j.atmosres.2021.105538

The box-whisker diagram plot in Figure 2 showed a clear seasonality (already observed in Table 1) with higher values in central months, with a high standard deviation specially at August due to African dust intrusions additionally to resuspension processes of local mineral aerosols owing to the dryness of the soil. Thus, the maximum AODs were found in summer and minimum values in winter. This evident AOD annual pattern is also found at seven sites in the Iberian Peninsula covering different aerosol types and environmental conditions during three coincident years (2010-2012) (Foyo-Moreno et al., 2019). The interquartile range P75-P25 is also larger in summer. It is worthy to note relatively high values of maximum AOD_{500} (0.66) and its P95 (0.21) in February. Despite of the low frequency of Saharan dust events over the Mediterranean region in winter (Gkikas et al., 2013, 2018; Querol et al., 2009), this is explained due to the intense Saharan dust events occurring in February 2016 and 2017 (Cazorla et al., 2017; Fernández et al., 2019), and also the increase in the anthropogenic local emissions in winter in addition to the orographic and meteorological conditions of Granada which favors the particle stagnation (Lyamani et al., 2012).

To study the interannual variability the box-wisher diagram plot of AOD_{500} at Granada is shown in Figure 3, for 2008-2018 years. The interannual range of AOD_{500} varies from 0.11 ± 0.08 in 2018 to 0.16 ± 0.14 in 2014 for, and showed firstly a decreasing trend in the subperiod 2008-2010, an increasing trend in 2010-2014 and a latter decreasing trend from 2014, but the Mann Kendall test revealed a slope of -0.001 with a p-value of 0.53 and, therefore, with no trend for AOD_{500}. The years with higher variability are 2012, 2015 and 2016, with a maximum difference between the extreme values for 2012. In general, a clear decrease in the aerosol load over the Iberian Peninsula has been observed since

https://doi.org/10.1016/j.atmosres.2021.105538

the 2000s. In particular, Mateos et al., 2015 found a decrease of -0.07 per decade in AOD_{400} for the Southeastern sector. Li et al. (2014) found a decreasing trend for a large stations number around the world (including Granada). Thus, the largest decreases were found over western Europe, reaching -0.1 per decade, and particularly they found at Granada a slope of -0.03 per decade for AOD_{400}. In our study, no significant trend has been found for AOD_{500} in the whole data.

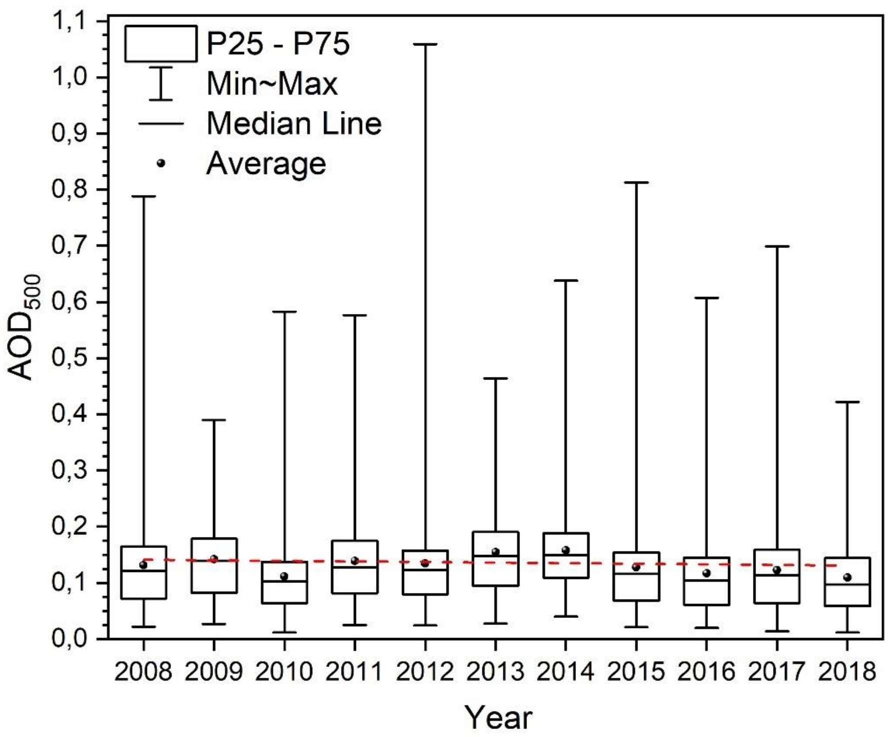

Figure 3. Annual statistics of AOD_{500} for the period 2008-2018. Bars correspond to the minimum and maximum values, the box limits are the P25 and P75 percentiles, the midline is the median and the sphere is the mean value. Dashed lines point out the linear trend evaluated by the Sen method.

4.2 Analysis of AFE and ARF

https://doi.org/10.1016/j.atmosres.2021.105538

Figure 4 shows the relationship between PAR and AOD_{500} for the entire studied period at different solar zenith angles centered at 15º, 30º, 45º, 60º and 75º (± 1º). For each year, five well-differentiated point clouds are observed, corresponding each of them to one of the five solar positions analyzed. As it was expected, the F_{net}^{PAR} increases for lower solar zenith angles due to the lower solar radiation path through the atmosphere at this solar position, increasing the solar irradiance reaching the surface. Additionally, a larger spread of the datapoints is observed for low values of AOD because of the large influence of the measurement uncertainty on the low AOD values. A similar behaviour has been observed for AFE^{total} (not shown here). An additional explanation of this datapoint large spread can be the existence of numerous sources of aerosols, which gives this region a high variability and complexity (Benavent-Oltra et al., 2017; Bravo-Aranda et al., 2015; Cazorla et al., 2017; Córdoba-Jabonero et al., 2011; Pérez-Ramírez et al., 2016).

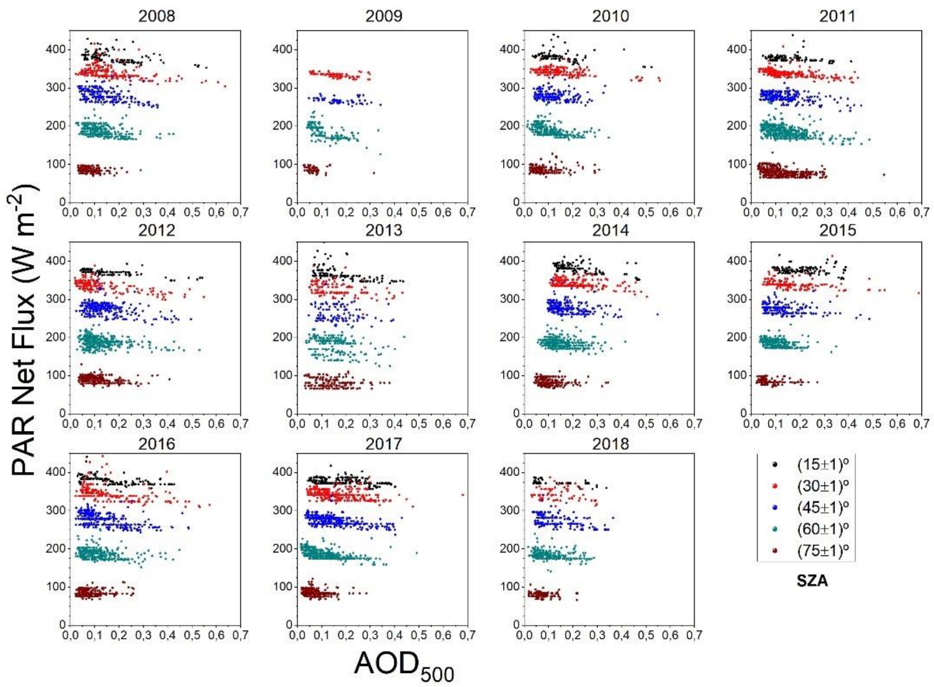

https://doi.org/10.1016/j.atmosres.2021.105538

Figure 4. Evolution of PAR Net Flux versus AOD_{500} for the period 2008-2018.

As it was described in Section 3.2, the slope of the linear fit at each angle category in Figure 4 represents the AFE. Both, AFE^{PAR} and AFE^{total} present negative values (Table 2), leading to a cooling effect by aerosols over Granada (Granados-Muñoz et al., 2019). AFE^{PAR} varies between -12 and -198 $Wm^{-2}\tau^{-1}$ while AFE^{total} ranges between -9 and -450 $Wm^{-2}\tau^{-1}$, showing a higher variability than in the PAR interval. These results agree with previous studies. Thus, Di Biagio et al. (2010) accounted for an AFE^{total} value of -309 ± 16 $Wm^{-2}\tau^{-1}$ for solar zenith angles between 15º and 25º and mixed aerosols at Lampedusa (Italy). Lower values have been estimated for other aerosol types as desert mineral dust and urban/industrial and biomass burning aerosols (Di Biagio et al., 2010). In this study, AFE^{PAR} entails between 20 and 60 % of the AFE^{total} with an average value of 30% for the whole dataset, which points out the relevance of the aerosol effects on PAR and the influence of this spectral interval.

Table 2. Surface aerosol forcing efficiency ($Wm^{-2}\tau^{-1}$) for PAR and Total irradiance (ARE^{PAR} and ARE^{total}, respectively) with its variability at one standard deviation level by years for different solar zenith angles (SZA).

	AFE^{PAR} ($Wm^{-2}\tau^{-1}$)				
	SZA (º)				
Year	15	30	45	60	75
2008	-65±12	-71±10	-103±14	-83±11	-28±11
2009		-47±8	-37±13	-198±18	-35±23
2010	-49±15	-52±5	-52±15	-117±12	1±11
2011	-27±13	-55±6	-75±8	-101±7	-49±6
2012	-43±4	-76±7	-80±10	-51±8	-36±8
2013	-92±15	-76±17	-50±30	-90±20	-27±13
2014	-78±10	-49±7	-69±12	-40±10	-17±9
2015	-18±9	-33±8	-53±11	-85±10	-12±9
2016	-64±8	-82±11	-94±9	-34±8	32±8

https://doi.org/10.1016/j.atmosres.2021.105538

2017	-27±5	-40±6	-74±5	-96±5	-40±8
2018	-42±1	-40±30	-83±13	-56±10	-24±14
	AFE^{total} ($Wm^{-2}\tau^{-1}$)				
	SZA (º)				
Year	15	30	45	60	75
2008	-170±30	-183±23	-300±30	-220±30	-30±40
2009		-220±30	-155±4	-450±50	-90±60
2010	-150±37	-144±17	-210±40	-330±40	-70±30
2011	-192±34	-168±18	-199±22	-281±19	-116±16
2012	-114±13	-163±18	-180±30	-123±19	-70±20
2013	-270±50	-200±50	-120±70	-220±60	-60±40
2014	-128±22	-126±23	-210±40	-210±30	-9±24
2015	-84±23	-92±18	-150±30	-310±30	-50±30
2016	-203±21	-200±30	-240±21	-205±23	59±21
2017	-149±13	-156±15	-219±12	-374±15	-170±30
2018	-170±19	-190±70	-310±40	-400±40	-120±60

Regarding the AFE dependence on solar zenith angle, both AFE^{PAR} and AFE^{total} showed enhanced values at roughly 45º or 60º. Other authors have reported a different pattern of this dependence with relatively constant or opposite trend for lower values of SZA and the same decreasing trend obtained in this work for high SZA values. Thus, Di Biagio et al. (2009) pointed out that this trend depends on the aerosol type and seems to be reversed for urban/industrial-biomass burning aerosols. Additionally, several authors suggested that the inflection point in this trend depends on the aerosol properties (Di Biagio et al., 2009, 2010; Formenti et al., 2002). This dependence of AFE on SZA can be explained by the combination of different factors. As the solar radiation path increases in the atmosphere, the attenuation as well as the diffuse fraction increases, especially at shorter wavelengths. On the other hand, for high SZA, the atmosphere is optically thicker and the AFE tends to decrease. Consequently, the AFE displays a dependence on SZA, which confirms the need to estimate forcing efficiency at fixed solar position applying the direct method employed in this study (Di Biagio et al., 2009, 2010; Formenti et al., 2002; Meloni et al., 2005; Nemesure et al., 1995).

https://doi.org/10.1016/j.atmosres.2021.105538

The same analysis has been carried out for the ARF. Table 3 shows the values for ARF^{PAR} and ARF^{total} during the full period, ranging from -1 to -23 Wm^{-2} and from -1 to -40 Wm^{-2} for ARF^{PAR} and ARF^{total}, respectively. These values are in accordance to those reported by other authors. Thus, Meloni et al. (2005) found ARF^{PAR} values between -10 and -20 Wm^{-2} at Lampedusa. Our work has reported a percentual ratio ARF^{PAR}/ARF^{total} of 50% in average, that is a higher value than the one found for AFE (30%). This average percentage found for ARF is higher than the mean value obtained at Granada for the ratio PAR to Total (43%) with values varying between 33 and 52% (Foyo-Moreno et al., 2017), highlighting the important role of the aerosols on PAR, greater than on Total. Following Ma et al. (2007), the ratio PAR to Total irradiance for various locations around the world present values between 35 and 58%.

Table 3. Surface aerosol radiative forcing (Wm^{-2}) for PAR and Total irradiance (ARF^{PAR} and ARF^{total}, respectively) with its variability at one standard deviation level by years for different solar zenith angles (SZA).

	ARF^{PAR} (Wm^{-2})				
	SZA (º)				
Year	15	30	45	60	75
2008	-11±9	-12±9	-15±10	-10±7	-2±2
2009	-	-8±4	-6±5	-23±14	-3±3
2010	-7±7	-8±6	-6±5	-13±8	0±1
2011	-5±4	-9±6	-10±7	-13±9	-6±4
2012	-6±5	-12±10	-11±8	-6±5	-4±3
2013	-15±11	-12±9	-9±8	-13±9	-4±4
2014	-17±8	-10±5	-12±6	-6±4	-2±2
2015	-4±3	-6±5	-7±6	-9±5	-1±1
2016	-11±8	-14±11	-12±9	-3±3	3±2
2017	-4±3	-7±4	-11±7	-10±7	-3±2
2018	-6±4	-5±6	-11±8	-6±4	-2±2
	ARF^{total} (Wm^{-2})				
	SZA (º)				
Year	15	30	45	60	75
2008	-21±19	-23±20	-31±25	-19±14	-2±3
2009	-	-26±13	-20±9	-40±30	-4±5

https://doi.org/10.1016/j.atmosres.2021.105538

2010	-15±17	-15±15	-18±14	-25±18	-4±4
2011	-24±20	-21±17	-20±17	-26±20	-9±7
2012	-14±14	-22±21	-19±17	-11±10	-5±5
2013	-30±30	-25±22	-15±17	-24±20	-6±7
2014	-21±13	-20±13	-27±16	-23±13	-1±2
2015	-12±10	-12±13	-14±13	-21±14	-2±3
2016	-28±24	-30±30	-24±22	-15±13	3±4
2017	-18±13	-20±14	-24±17	-27±22	-7±5
2018	-16±14	-18±19	-30±24	-30±30	-5±6

Regarding the dependence of ARF on solar position, a similar pattern to that of AFE is found. The absolute ARF values increase with increasing SZA up to 45º or 60º, depending on the year considered, and then decrease. However, this dependence is less pronounced than for AFE, with values relatively constant for SZA below an intermediate value. The value of SZA for the change always is coinciding with the values obtained for AFE and also is coinciding for PAR and Total irradiance except for 2018. This trend is similar to that obtained by Meloni et al. (2005), but the trend is reversed for aerosols more absorbing. This fact may explain the different behavior below a given SZA value. Our work covers a long period including a wide variety of aerosols and, thus, this mixture generally exhibits large values of single scattering albedo. In fact, the maximum values of single scattering albedo registered at Granada during the years 2010-2012 are close to 1, which indicates that Granada recorded events of non-absorbing aerosols (Foyo-Moreno et al., 2019).

Comparing our results with previous studies, we found similar values of both AFE and ARF for both PAR and Total irradiance. Antón et al. (2012) performed ARF and AFE calculations at Granada for Total irradiance with another method and they found, values of ARF between -100 and -200 Wm^{-2} and AFE of -115 $Wm^{-2}\tau^{-1}$ at 675 nm during an African dust event. For a longer period of time (2005-2010), Valenzuela et al. (2012) computed values of ARF and AFE with the radiative transfer model SBDART during African dust

https://doi.org/10.1016/j.atmosres.2021.105538

events, and found ARF from -13 to -34 Wm^{-2} and AFE from -65 to -74 $Wm^{-2}\tau^{-1}$ at 440 nm, depending on the mineral sources. Foyo-Moreno et al. (2014), using the direct method for the radiative effects calculations, found an ARF of -28 Wm^{-2} and an AFE of -73.4 $Wm^{-2}\tau^{-1}$ at solar fixed angle of 15º during the period 2006-2007. Focusing on PAR Lyamani et al. (2006b) found values of ARF of -20.4 $Wm^{-2}\tau^{-1}$ during an African dust event in 2003 and -16.1 Wm^{-2} during intrusions from the Central Europe region, with AFE values of -73.4 and -78.2 $Wm^{-2}\tau^{-1}$ at 670 nm. Therefore, all these studies, performed in the same area of study, found values that are within the ranges of our findings. Other authors focused on other regions of the Mediterranean basin. Meloni et al. (2005), using a radiative transfer model at 400-700 nm, found ARF daily mean values -12.9 and -19.5 Wm^{-2} in July and AFE at 500 nm ranging between -28.4 and -30.1 $Wm^{-2}\tau^{-1}$ and between -42.9 and -45.6 $Wm^{-2}\tau^{-1}$ for several days at Lampedusa. Sicard et al. (2016) for 50º < SZA <60º found values of ARF^{total} of (-23 ± 13) Wm^{-2} and (-136 ± 41) $Wm^{-2}\tau^{-1}$ for AFE^{total} in summer at Palma de Mallorca (Mallorca Island, Spain). All of these values are in good agreement with our findings.

However, it is necessary to emphasize the different methodologies used in the works of most of the authors, deriving ARF from radiative transfer model calculation and obtaining averages daily values, whose calculations require aerosol information not known a priori. Thus, in a few cases instantaneous direct measurements of the net fluxes have been used to derive ARF, and further the effects of atmospheric aerosols on PAR scarcely have been studied.

https://doi.org/10.1016/j.atmosres.2021.105538

4.3 Analysis of AFE and ARF trends

Figures 5b and 6b show the pattern followed for AFE and ARF, with an inflexion point at 60^{o} for both PAR and Total irradiance, showing a similar pattern as described in section 4.2. This similar pattern is explained by the long path at high solar zenith angle, which includes strong attenuation of direct solar radiation but also more multiple scattering and hence more scattered light (Lyamani et al., 2006b). The dependence on SZA is more pronounced for ARF with respect to AFE. In spite of this growth pattern, values of AFE and ARF are close to be constant for angles smaller than 45^{o} for both Total and PAR, and this finding are in agreement with previous studies for surface AFE estimated by radiative transfer model simulations (Formenti et al., 2002; Meloni et al., 2005). On the other hand, analyzing ARF^{PAR} and AFE^{PAR} by years, absolute terms, maximum values have been found in 2008 and 2009 (-10 Wm^{-2}, -79 $Wm^{-2}\tau^{-1}$), and minimum values of -5.3 Wm and -41 $Wm^{-2}\tau^{-1}$ (ARF and AFE, respectively) both in 2015. For Total radiation maximum values are obtained in 2009 and 2018 (-22 Wm^{-2} and -239 $Wm^{-2}\tau^{-1}$), and minimum values in 2015 (-12 Wm^{-2} and -136 $Wm^{-2}\tau^{-1}$) (Figures 5a and 6a).

https://doi.org/10.1016/j.atmosres.2021.105538

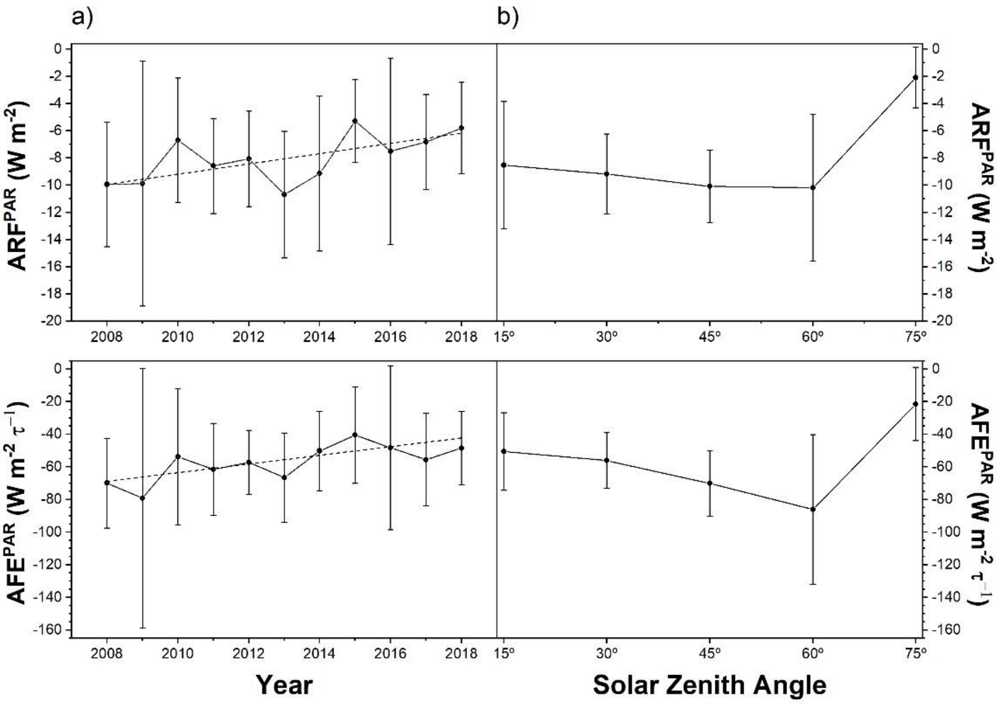

Figure 5. Evolution of surface aerosol radiative forcing for PAR (ARF^{PAR}) and surface aerosol forcing efficiency for PAR (AFE^{PAR}) with its variability at one standard deviation level by years and solar zenith angle (SZA). Dashed lines point out the linear trends evaluated by the Sen method.

The trends analyses revealed for ARF^{PAR} and AFE^{PAR} (considering absolute values) a downward trend for 2008-2018 period with a slope of 0.38 $Wm^{-2}year^{-1}$ and 2.66 $Wm^{-2}\tau^{-1}year^{-1}$, respectively, being significant for AFE with a p-value < 0.05 and very close to being significant for ARF (p-value = 0.062) (Figure 6a). Although the slope is positive, taking into account that the ARF (and AFE) values are negative, the slope value implies that the aerosol cooling radiative effect of aerosols is decreasing. The influence of calibration factor changes on this trend is negligible based on the long-term stability estimated for the PAR sensor along the analyzed period and described in Section 2. This result is interesting considering the decrease trend detected for AOD in the last years

https://doi.org/10.1016/j.atmosres.2021.105538

already commented in section 4.1. However, no upward or downward trend has been observed for the annual evolution of ARF^{total} and AFE^{total} (Figure 6a). In order to consider a potential compensating effect of other spectral ranges, we have performed the calculation also with Total minus PAR, i.e. ultraviolet A and B plus near-infrared irradiance, and no statistically significant trend was found, although the slope is of opposite sign. This result can be attributed to aerosol properties especially to the aerosol absorption characteristics. In fact, AFE exhibits a dependence on single scattering albedo and a larger contribution of the PAR range in relation to Total irradiance is found for high absorbing aerosols (Mateos et al. 2014). These results indicate the importance of the knowledgement of the PAR, because it is more sensitive to atmospheric aerosol effects than Total irradiance and, however, it has not been implemented nowadays at most radiometric stations instruments to measure routinely the PAR irradiance, unlike Total irradiance, which is a standard variable measured at the Baseline Surface Radiation Network (BSRN) and many other radiometric stations.

https://doi.org/10.1016/j.atmosres.2021.105538

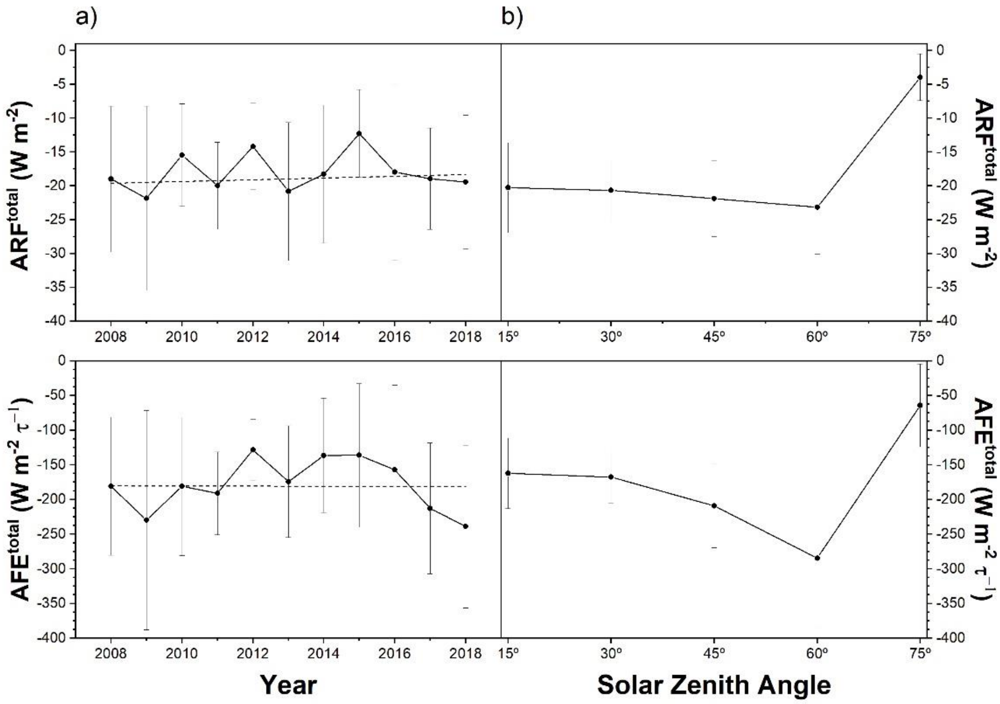

Figure 6. Evolution of surface aerosol radiative forcing for total irradiance (ARF^{total}) and surface aerosol forcing efficiency for total irradiance (AFE^{total}) with its variability at one standard deviation level by years and solar zenith angle (SZA). Dashed lines point out the linear trends evaluated by the Sen method.

5. CONCLUSIONS

Eleven years data set period were analyzed to determine the aerosols radiative effects in the photosynthetically active radiation (PAR; 400-700 nm) and Total irradiance (280-3000 nm) over an urban site located in a mid-latitude in the Western Mediterranean region. These effects have been analyzed through the estimation of aerosol forcing efficiency (AFE) and aerosol radiative forcing (ARF), using the direct method, obtaining instantaneous values from experimental measurements of aerosol optical depth (AOD)

https://doi.org/10.1016/j.atmosres.2021.105538

and irradiance measurements. The advantage of this method unlike other methods using radiative model calculations is that it does not require aerosol information. The main conclusions are:

1. A seasonal evolution has been found with maximum AOD_{500} values in summer (0.16 ± 0.09), corresponding to the highest incidence of Saharan dust events and minimum ones in winter (0.08 ± 0.04). The AFE values ranged between (-12 ± 9) $Wm^{-2}\tau^{-1}$ and (-198 ± 18) $Wm^{-2}\tau^{-1}$ for PAR while for Total the values varied from (-9 ± 24) $Wm^{-2}\tau^{-1}$ and (-450 ± 50) $Wm^{-2}\tau^{-1}$, meanwhile ARF values ranged from (-1±1) Wm^{-2} and (-23 ± 14) Wm^{-2} in the case of PAR and from (-1 ± 2) Wm^{-2} to (-40 ± 30) Wm^{-2} for Total.
2. A dependence of both AFE and ARF on solar zenith angle was found with a clear pattern increasing values of ARF and AFE (in absolute sense) for increasing SZA, and an inflexion point at 45°-60° range.
3. The percentage of ARF for PAR with respect to Total irradiance had a mean value of 50%, a higher value than that obtained for AFE (30%), evidencing the important impact of atmospheric aerosols on PAR because the ratio PAR/Total irradiance had a lower average value (43%).
4. A downward trend for AFE for PAR was found with a slope of 2.7 $Wm^{-2}\tau^{-1}year^{-1}$ with a p-value < 0.05 and no significative trend was found for Total irradiance, demonstrating that PAR is more sensitive to atmospheric aerosols effects than Total irradiance and, therefore, evidencing the need to increase the knowledge of PAR and its interaction with atmospheric aerosols.

https://doi.org/10.1016/j.atmosres.2021.105538

5. The contribution of different spectral ranges in the trend analysis for AFE can be governed by the aerosol type, being in general, the visible spectral range the most dominant, with a variable contribution depending on the aerosol type.

ACKNOWDLEGMENTS This work was supported by the Spanish Ministry of Economy and Competitiveness through projects CGL2016-81092-R, CGL2017-90884-REDT and RTI2018.101154.A.I00, by the Andalusia Regional Government, University of Granada and FEDER funds through projects B-RNM-496-UGR18 and P18-RT-3820, and by the Spanish Ministry of Education, Culture and Sport through grant FPU15/05436. The financial support in the ACTRIS Research Infrastructure Project by the European Union's Horizon 2020 research and innovation program through project ACTRIS-2 (grant agreement No 654109) and ACTRIS-IMP (grant agreement No 871115). The authors thankfully acknowledge the FEDER program for the instrumentation used in this work and the University of Granada that supported this study through the Excellence Units Program.

REFERENCES

Akitsu, T., Nasahara, K. N., Hirose, Y., Ijima, O., Kume, A., 2017. .Quantum sensors for accurate and stable long-term photosynthetically active radiation observations. Agr. For. Meteor., 237-238, 171-183. https://doi.org/10.1016/j.agrformet.2017.01.011

Alados, I., Foyo-Moreno, I., Alados-Arboledas, L., 1996. Photosynthetically active radiation: Measurements and modelling. Agric. For. Meteor., 78, 121-131. https://doi.org/10.1016/0168-1923(95)02245-7.

Alados-Arboledas, L., Müller, D., Guerrero-Rascado, J. L., Navas-Guzmán, F., Pérez-Ramírez, D., Olmo, F. J., 2011. Optical and microphysical properties of fresh biomass burning aerosol retrieved by Raman lidar, and star-and sun-photometry. J. Geophys. Res. Letters, 38. https://doi.org/10.1029/2010GL045999.

Alados-Arboledas, L., Olmo, F. J., Alados, I., Pérez, M., 2000. Parametric models to estimate photosynthetically active radiation in Spain. Agric. For. Meteor., 101, 187-201. https://doi.org/10.1016/S0168-1923(99)00163-X.

Andreae, M. O., Jones, C. D., Cox, P. M., 2005. Strong present-day aerosol cooling implies a hot future. Nature, 435, 1187–1190.

Antón, M., Gil, J. E., Fernández-Gálvez, J., Lyamani, H., Valenzuela, A., Foyo-Moreno, I., Olmo, F. J., Alados-Arboledas, L., 2011. Evaluation of the aerosol forcing efficiency in the UV erythemal range at Granada, Spain. n. J. Geophys. Res-Atmos., 116(D20), D20214. https://doi.org/10.1029/2011JD016112.

Antón, M., Valenzuela, A., Cazorla, A., Gil, J. E., Fernández-Gálvez, J., Lyamani, H., Foyo-Moreno, I., Olmo, F. J., Alados-Arboledas, L., 2012. Global and diffuse shortwave irradiance during a strong desert dust episode at Granada (Spain). Atmos. Res., 118, 232-239. https://doi.org/10.1016/j.atmosres.2012.07.007.

Baars, H., Ansmann, A., Ohneiser, K., Haarig, M., Engelmann, R., Althausen, D., Hanssen, I., Gausa, M., Pietruczuk, A., Szkop, A., Stachlewska, I. S., Wang, D., Reichardt, J., Skupin, A., Mattis, I., Trickl, T., Vogelmann, H., Navas-Guzmán, F., Haefele, A., Pappalardo, G., 2019. The unprecedented 2017-2018 stratospheric smoke event: Decay phase and aerosol properties observed with the EARLINET. Atmos. Chem. Phys., 19 (23), 15183-15198. https://doi.org/10.5194/acp-19-15183-2019.

https://doi.org/10.1016/j.atmosres.2021.105538

Benavent-Oltra, J. A., Román, R., Granados-Muñoz, M. J., Pérez-Ramírez, D., Ortiz-Amezcua, P., Denjean, C., Lopatin, A., Lyamani, H., Torres, B., Guerrero-Rascado, J. L., Fuertes, D., Dubovik, O., Chaikovsky, A., Olmo, F. J., Mallet, M., Alados-Arboledas, L., 2017. Comparative assessment of GRASP algorithm for a dust event over Granada (Spain) during ChArMEx-ADRIMED 2013 campaign. Atmos. Meas. Tech., *10*(11), 4439-4457. https://doi.org/10.5194/amt-10-4439-2017.

Bennouna, Y.S., Cachorro, V.E. Mateos, D., Burgos, M.A., Toledano, C., Torres, B. , A.M. de Frutos, A.M., 2016. Long-term comparative study of columnar and surface mass concentration aerosol properties in a background environment. Atmos. Env., 140, 261-272.

Bergstrom, R. W., Pilewskie, P., Russell, P. B., Redemann, J., Bond, T. C., Quinn, P. K., Sierau, B., 2007. Spectral absorption properties of atmospheric aerosols. Atmos. Chem. and Phys. Discuss., 7(4), 10669-10686.

Bravo-Aranda, J. A., Titos, G., Granados-Muñoz, M. J., Guerrero-Rascado, J. L., Navas-Guzmán, F., Valenzuela, A., Lyamani, H., Olmo, F. J., Andrey, J., Alados-Arboledas, L., 2015. Study of mineral dust entrainment in the planetary boundary layer by lidar depolarisation technique. Tellus B: Chem. and Phys. Meteor. 67(1), 26180. https://doi.org/10.3402/tellusb.v67.26180.

Buffoni, L., Maugeri, M., Nanni, T., 1999. Precipitation in Italy from 1833 to 1996. Theo. and App. Clim., 63 (1-2), 33–40.

Bush, B. C., Valero, F. P. J., 2003. Surface aerosol radiative forcing at Gosan during the ACE-Asia campaign. J. Geophys. Res. Atmos., 108 (D23). https://doi.org/10.1029/2002JD003233.

https://doi.org/10.1016/j.atmosres.2021.105538

Cariñanos, P., Foyo-Moreno, I., Alados, I., Juan Luis Guerrero-Rascado, J.L., Ruiz-Peñuela, S., Titos, G., Cazorla A., Alados-Arboledas, L., Díaz de la Guardia, C., 2021. Bioaerosols in urban environments: Trends and interactions with pollutants and meteorological variables based on quasi-climatological series. J. of Env. Manag. 282, 111963. https://doi.org/10.1016/j.jenvman.2021.111963.

Caya, M. V. C., Alcantara, J. T., Carlos, J. S., Cereno, S. S. B., 2018. Photosynthetically active radiation (PAR) sensor using an array of light sensors with the integration of data logging for agricultural application. *2018 3rd International Conference on Computer and Communication Systems (ICCCS)*, 377–381.

Cazorla, A., Casquero-Vera, J. A., Román, R., Guerrero-Rascado, J. L., Toledano, C., Cachorro, V. E., Orza, J. A. G., Cancillo, M. L., Serrano, A., Titos, G., Pandolfi, M., Alastuey, A., Hanrieder, N., Alados-Arboledas, L., 2017. Near-real-time processing of a ceilometer network assisted with sun-photometer data: Monitoring a dust outbreak over the Iberian Peninsula. Atmos. Chem. and Phys., 17(19), 11861-11876. https://doi.org/10.5194/acp-17-11861-2017.

Charlson, R. J., Langner, J., Rodhe, H., Leovy, C. B., Warren, S. G., 1991. Perturbation of the northern hemisphere radiative balance by backscattering from anthropogenic sulfate aerosols. Tellus A: Dynamic Meteorol. and Oceano., 43(4), 152–163.

Córdoba-Jabonero, C., Sorribas, M., Guerrero-Rascado, J. L., Adame, J. A., Hernández, Y., Lyamani, H., Cachorro, V., Gil, M., Alados-Arboledas, L., Cuevas, E., de la Morena, B., 2011. Synergetic monitoring of Saharan dust plumes and potential impact on surface: A case study of dust transport from Canary Islands to Iberian Peninsula. Atmos. Chem. and Phys., 11(7), 3067-3091. https://doi.org/10.5194/acp-11-3067-2011.

https://doi.org/10.1016/j.atmosres.2021.105538

Da Silva, V. de P. R., e Silva, R. A., Cavalcanti, E. P., Braga, C. C., de Azevedo, P. V., Singh, V. P., Pereira, E. R. R., 2010. Trends in solar radiation in NCEP/NCAR database and measurements in northeastern Brazil. Sol. Energ., 84(10), 1852–1862.

Dadashi-Roudbari, A., Ahmadi, M., 2020. Evaluating temporal and spatial variability and trend of aerosol optical depth (550 nm) over Iran using data from MODIS on board the Terra and Aqua satellites. *Arabian* J. of Geosciences, 13(6), 1-23. https://doi.org/10.1007/s12517-020-5232-0.

Di Biagio, C., di Sarra, A., Meloni, D., 2010. Large atmospheric shortwave radiative forcing by Mediterranean aerosols derived from simultaneous ground-based and spaceborne observations and dependence on the aerosol type and single scattering albedo. J. of Geophys. Res., 115 (D10), D10209. https://doi.org/10.1029/2009JD012697.

Di Biagio, C., di Sarra, A., Meloni, D., Monteleone, F., Piacentino, S., Sferlazzo, D., 2009. Measurements of Mediterranean aerosol radiative forcing and influence of the single scattering albedo. J. Geophys. Res., 114(D6), D06211. https://doi.org/10.1029/2008JD011037.

Díaz, A. M., García, O. E., Díaz, J. P., Expósito, F. J., Utrillas, M. P., Martínez-Lozano, J. A., Alados-Arboledas, L., Olmo, F. J., Lorente, J., Cachorro, V., Horvath, H., Labajo, A., Sorribas, M., Vilaplana, J. M., Silva, A. M., Elias, T., Pujadas, M., Rodrigues, J. A., González, J. A., 2007. Aerosol radiative forcing efficiency in the UV region over southeastern Mediterranean: VELETA2002 campaign. J. Geophys. Res., 112(D6), D06213. https://doi.org/10.1029/2006JD007348.

https://doi.org/10.1016/j.atmosres.2021.105538

Esteve, A. R., Estellés, V., Utrillas, M. P., Martínez-Lozano, J. A., 2012. In-situ integrating nephelometer measurements of the scattering properties of atmospheric aerosols at an urban coastal site in western Mediterranean. Atmos. Environ., 47, 43–50.

Eswaran, K., Satheesh, S. K., Srinivasan, J., 2019. Sensitivity of aerosol radiative forcing to various aerosol parameters over the Bay of Bengal. J. of Earth System Scien., 128 (6), 170. https://doi.org/10.1007/s12040-019-1200-z.

Farahat, A., El-Askary, H., Adetokunbo, P., Fuad, A.T., 2016. Analysis of aerosol absorption properties and transport over North Africa and the Middle East using AERONET data. Ann. Geophy., 34(11), 1031-1044. https://doi.org/10.5194/angeo-34-1031-2016.

Fernández, A. J., Sicard, M., Costa, M. J., Guerrero-Rascado, J. L., Gómez-Amo, J. L., Molero, F., Barragán, R., Basart, S., Bortoli, D., Bedoya-Velásquez, A. E., 2019. Extreme, wintertime Saharan dust intrusion in the Iberian Peninsula: Lidar monitoring and evaluation of dust forecast models during the February 2017 event. Atmos. Res., 228, 223–241.

Formenti, P., Boucher, O., Reiner, T., Sprung, D., Andreae, M. O., Wendisch, M., Wex, H., Kindred, D., Tzortziou, M., Vasaras, A., Zerefos, C., 2002. STAAARTE-MED 1998 summer airborne measurements over the Aegean Sea 2. Aerosol scattering and absorption, and radiative calculations. J. Geophys. Res. Atmos., *107*(D21), AAC 2-1-AAC 2-14. https://doi.org/10.1029/2001JD001536.

Foyo-Moreno, I., Alados, I., Alados-Arboledas, L., 2017. A new conventional regression model to estimate hourly photosynthetic photon flux density under all sky conditions: Int. J. Clim., *37*, 1067-1075. https://doi.org/10.1002/joc.5063.

Foyo-Moreno, I., Alados, I., Antón, M., Fernández-Gálvez, J., Cazorla, A., Alados-Arboledas, L., 2014. Estimating aerosol characteristics from solar irradiance measurements at an urban location in southeastern Spain: Aerosol properties from solar irradiance. J. Geophys. Res. Atmos., 119(4), 1845-1859. https://doi.org/10.1002/2013JD020599.

Foyo-Moreno, I., Alados, I., Guerrero-Rascado, J. L., Lyamani, H., Pérez-Ramírez, D., Olmo, F. J., Alados-Arboledas, L., 2019. Contribution to column-integrated aerosol typing based on Sun-photometry using different criteria. Atmos. Res., 224, 1–17. https://doi.org/10.1016/j.atmosres.2019.03.007.

García, O. E., Díaz, A. M., Expósito, F. J., Díaz, J. P., Gröbner, J., Fioletov, V. E., 2006. Cloudless aerosol forcing efficiency in the UV region from AERONET and WOUDC databases. Geophys. Res. Lett., 33(23), L23803. https://doi.org/10.1029/2006GL026794.

Garcia-Herrera, R. F., Lionello, P., Ulbrich, U., 2014. Preface: Understanding dynamics and current developments of climate extremes in the Mediterranean region. Nat. Hazards Earth Syst. Sci., 8.

Ge, S., Smith, R. G., Jacovides, C. P., Kramer, M. G., Carruthers, R. I., 2011. Dynamics of photosynthetic photon flux density (PPFD) and estimates in coastal northern California. Theor.App. Clim-., 105(1-2), 107-118. https://doi.org/10.1007/s00704-010-0368-6.

Giles, D. M., Sinyuk, A., Sorokin, M. G., Schafer, J. S., Smirnov, A., Slutsker, I., Eck, T. F., Holben, B. N., Lewis, J. R., Campbell, J. R., Welton, E. J., Korkin, S. V., Lyapustin, A. I., 2019. Advancements in the Aerosol Robotic Network (AERONET) Version 3 database – automated near-real-time quality control algorithm with improved cloud screening for

Sun photometer aerosol optical depth (AOD) measurements. Atmos. Meas. Tech., 12(1), 169-209. https://doi.org/10.5194/amt-12-169-2019.

Gkikas, A., Hatzianastassiou, N., Mihalopoulos, N., Katsoulis, V., Kazadzis, S., Pey, J., Querol, X., Torres, O., 2013. The regime of intense desert dust episodes in the Mediterranean based on contemporary satellite observations and ground measurements. Atmos. Chem. and Phys., 13(23), 12135-12154. https://doi.org/10.5194/acp-13-12135-2013.

Gkikas, A., Obiso, V., Pérez García-Pando, C., Jorba, O., Hatzianastassiou, N., Vendrell, L., Basart, S., Solomos, S., Gassó, S., Baldasano, J. M., 2018. Direct radiative effects during intense Mediterranean desert dust outbreaks. Atmos. Chem. and Phys., *18*(12), 8757-8787. https://doi.org/10.5194/acp-18-8757-2018.

Gopal, K. R., Arafath, S. M., Lingaswamy, A. P., Balakrishnaiah, G., Kumari, S. P., Devi, K. U., Reddy, N. S. K., Reddy, K. R. O., Reddy, M. P., Reddy, R. R., 2014. In-situ measurements of atmospheric aerosols by using Integrating Nephelometer over a semi-arid station, southern India. Atmos. Env., 86, 228–240.

Granados-Muñoz, M. J., Sicard, M., Román, R., Benavent-Oltra, J. A., Barragán, R., Brogniez, G., Denjean, C., Mallet, M., Formenti, P., Torres, B., 2019. Impact of mineral dust on shortwave and longwave radiation: Evaluation of different vertically resolved parameterizations in 1-D radiative transfer computations. Atmos. Chem. and Phys., 19(1), 523–542. https://doi.org/10.5194/acp-19-523-2019.

Guerrero-Rascado, J. L., Olmo, F. J., Avilés-Rodríguez, I., Navas-Guzmán, F., Pérez-Ramírez, D., Lyamani, H., Alados Arboledas, L., 2009. Extreme Saharan dust event over the southern Iberian Peninsula in september 2007: Active and passive remote sensing from surface and satellite. Atmos. Chem. and Phys., 9(21), 8453-8469. https://doi.org/10.5194/acp-9-8453-2009.

Guerrero-Rascado, J. L., Ruiz, B., Alados-Arboledas, L., 2008. Multi-spectral Lidar characterization of the vertical structure of Saharan dust aerosol over southern Spain. Atmos. Env., 42(11), 2668-2681. https://doi.org/10.1016/j.atmosenv.2007.12.062

Hansen, J., Sato, M., Kharecha, P., Von Schuckmann, K., 2011. Earth’s energy imbalance and implications. Atmos. Chem. and Phys., *11(24)*, 13421-13449. https://doi.org/10.5194/acp-11-13421-2011.

Holben, B. N., Eck, T. F., Slutsker, I., Tanré, D., Buis, J. P., Setzer, A., Vermote, E., Reagan, J. A., Kaufman, Y. J., Nakajima, T., Lavenu, F., Jankowiak, I., Smirnov, A., 1998. AERONET—A Federated Instrument Network and Data Archive for Aerosol Characterization. Rem. Sens.of Env., 66(1), 1-16. https://doi.org/10.1016/S0034-4257(98)00031-5.

Iqbal, M. 1983. An Introduction to Solar Radiation. Academic Press: London.

Jeff Burkey., 2020. Mann-Kendall Tau-b with Sen's Method (enhanced) (https://www.mathworks.com/matlabcentral/fileexchange/11190-mann-kendall-tau-b-with-sen-s-method-enhanced), MATLAB Central File Exchange. Retrieved December 23, 2020https://www.mathworks.com/matlabcentral/fileexchange/11190-mann-kendall-tau-b-with-sen-s-method-enhanced.

Jonard, F., De Cannière, S., Brüggemann, N., Gentine, P., Short Gianotti, D. J., Lobet, G., Miralles, D. G., Montzka, C., Pagán, B. R., Rascher, U., Vereecken, H., 2020. Value of sun-induced chlorophyll fluorescence for quantifying hydrological states and fluxes: Current status and challenges. Agr. and For. Meteor., *291*, 108088. https://doi.org/10.1016/j.agrformet.2020.108088.

Kodera, K., Hori, M. E., Yukimoto, S., Sigmond, M., 2008. Solar modulation of the Northern Hemisphere winter trends and its implications with increasing CO2. Geophys. Research Letters, 35(3).

Kuo, C.-C., Gan, T. Y., Wang, J., 2020. Climate change impact to Mackenzie river Basin projected by a regional climate model. Clim. Dyn., 54(7), 3561-3581. https://doi.org/10.1007/s00382-020-05177-7.

Li, L., Li, Z., Chang, W., Ou, Y., Goloub, P., Li, C., Li, K., Hu, Q., Wang, J., Wendisch, M. 2020. Aerosol solar radiative forcing near the Taklimakan Desert based on radiative transfer and regional meteorological simulations during the Dust Aerosol Observation-Kashi campaign. Atmos. Chem. and Phys., 20(18), 10845-10864. https://doi.org/10.5194/acp-20-10845-2020.

Lionello, P., Abrantes, F., Gacic, M., Planton, S., Trigo, R., Ulbrich, U., 2014. The climate of the Mediterranean region: Research progress and climate change impacts. Reg. Env. Change, 14(5), 1679-1684. https://doi.org/10.1007/s10113-014-0666-0.

Lyamani, H., Fernandez-Galvez, J., Perez-Ramirez, D., Valenzuela, A., Anton, M., Alados, I., Titos, G., Olmo, F. J., Alados-Arboledas, L., 2012. Aerosol properties over two urban sites in South Spain during an extended stagnation episode in winter season. Atmos. Env., 62, 424-432. https://doi.org/10.1016/j.atmosenv.2012.08.050.

https://doi.org/10.1016/j.atmosres.2021.105538

Lyamani, H., Olmo, F. J., Alados-Arboledas, L., 2010. Physical and optical properties of aerosols over an urban location in Spain: Seasonal and diurnal variability. Atmos. Chem. and Phys., 10, 239-254.

Lyamani, H., Olmo, F. J., Alcántara, A., Alados-Arboledas, L., 2006a. Atmospheric aerosols during the 2003 heat wave in southeastern Spain I: Spectral optical depth. Atmos. Env., 40(33), 6453-6464. https://doi.org/10.1016/j.atmosenv.2006.04.048.

Lyamani, H., Olmo, F. J., Alcántara, A., Alados-Arboledas, L., 2006b. Atmospheric aerosols during the 2003 heat wave in southeastern Spain II: Microphysical columnar properties and radiative forcing. Atmos. Env., 40(33), 6465-6476. https://doi.org/10.1016/j.atmosenv.2006.04.047.

Ma, J., Liu, J., Li, S., Liang, H., Jiang, C. Y., Wang, B. Z., 2007. Study on the features of the photosynthetic active radiation (PAR) with experimentations and measurements. J. of Nat. Resources, 22 (5), 673-682. http://dx.doi.org/10.11849/zrzyxb.2007.05.001.

Mann, H. B. 1945. Nonparametric Tests Against Trend. Econometrica, *13*(3), 245-259. JSTOR. https://doi.org/10.2307/1907187.

Li, J., Carlson, B.E., Dubovik, O., Lacis, A.A., 2014. Recent trends in aerosol optical properties derived from AERONET measurements. Atmos. Chem. Phys. 14, 12271–12289. http://dx.doi.org/10.5194/acp-14-12271-2014.

Mateos, D., Antón, M., Toledano, C., Cachorro, V. E., Alados-Arboledas, L., Sorribas, M., Costa, M. J., Baldasano, J. M., 2014. Aerosol radiative effects in the ultraviolet, visible, and near-infrared spectral ranges using long-term aerosol data series over the Iberian

https://doi.org/10.1016/j.atmosres.2021.105538

Peninsula. Atmos. Chem. and Phys., 14(24), 13497-13514. https://doi.org/10.5194/acp-14-13497-2014.

Mateos, D., Cachorro, V. E., Toledano, C., Burgos, M.A., Bennouna, Y., Torres, B., Fuertes, D., Gonzalez, R., Guirado, C., Calle, A., de Frutos., 2015. Columnar and surface aerosol load over the Iberian Peninsula establishing annual cycles, trends, and relationships in five geographical sectors. The Scien. of the Total Env., 518-519, 378-392.

McCree, K. J., 1972. Test of current definitions of photosynthetically active radiation against leaf photosynthesis data. Agr. Meteor., *10*, 443-453. https://doi.org/10.1016/0002-1571(72)90045-3.

McCree, K. J., 1981. Photosynthetically Active Radiation. En O. L. Lange, P. S. Nobel, C. B. Osmond, & H. Ziegler (Eds.), Physiological Plant Ecology I (pp. 41-55). Springer Berlin Heidelberg. https://doi.org/10.1007/978-3-642-68090-8_3.

Meloni, D., di Sarra, A., Di Iorio, T., Fiocco, G., 2005. Influence of the vertical profile of Saharan dust on the visible direct radiative forcing. J- of Quantitative Spectroscopy and Rad. Transfer, 93(4), 397-413. https://doi.org/10.1016/j.jqsrt.2004.08.035.

Nabat, P., Somot, S., Mallet, M., Sevault, F., Marc Chiacchio, M., Wild, M., 2015. Direct and semi-direct aerosol radiative effect on the Mediterranean climate variability using a coupled regional climate system model. Clym. Dyn., 44, 1127-1155.

Navas-Guzmán, F., Müller, D., Bravo-Aranda, J. A., Guerrero-Rascado, J. L., Granados-Muñoz, M. J., Pérez-Ramírez, D., Olmo, F. J., Alados-Arboledas, L., 2013. Eruption of the Eyjafjallajökull Volcano in spring 2010: Multiwavelength Raman lidar measurements of sulphate particles in the lower troposphere. J. of Geophys. Res.: Atmos., *118*(4), 1804-1813. https://doi.org/10.1002/jgrd.50116.

Nemesure, S., Wagener, R., Schwartz, S. E., 1995. Direct shortwave forcing of climate by the anthropogenic sulfate aerosol: Sensitivity to particle size, composition, and relative humidity. J. of Geophys. Res., 100(D12), 26,105-26,116. Scopus. https://doi.org/10.1029/95jd02897.

Obregón, M. A., Costa, M.J.; Serrano, A., Silva A.M., 2017. A. Thirteen Years of Aerosol Radiative Forcing in Southwestern Iberian Peninsula. Aerosol Air Qual. Res. 2017, 17, 2509–2521.

Obregón, M. A., Costa, M.J.; Silva A.M.; Serrano, A., 2020. Spatial and Temporal Variation of Aerosol and Water Vapour Effects on Solar Radiation in the Mediterranean Basin during the Last Two Decades. Remote Sens., 12, 1316; https://doi:10.3390/rs12081316.

Olmo, F. J., Alados-Arboledas, L., 1995. Pinatubo eruption effects on solar radiation at Almeria (36.83 N, 2.41 W). Tellus B: Chem. and Phys.l Meteorol., 47(5), 602–606.

Ortiz-Amezcua, P., Guerrero-Rascado, J. L., Granados-Muñoz, M. J., Bravo-Aranda, J. A., Alados-Arboledas, L., 2014. Characterization of atmospheric aerosols for a long range transport of biomass burning particles from canadian forest fires over the southern iberian peninsula in July 2013. Óptica Pura y Aplicada, 47(1), 43–49.

Ortiz-Amezcua, P., Guerrero-Rascado, J. L., Granados-Muñoz, M. J., Benavent-Oltra, J. A., Böckmann, C., Samaras, S., Stachlewska, I. S., Janicka, Ł., Baars, H., Bohlmann, S., Alados-Arboledas, L., 2017. Microphysical characterization of long-range transported

https://doi.org/10.1016/j.atmosres.2021.105538

biomass burning particles from North America at three EARLINET stations. Atmos. Chem. and Phys., 17(9), 5931-5946. https://doi.org/10.5194/acp-17-5931-2017.

Pérez-Ramírez, D., Lyamani, H., Smirnov, A., O'Neill, N. T., Veselovskii, I., Whiteman, D. N., Olmo, F. J., Alados-Arboledas, L., 2016. Statistical study of day and night hourly patterns of columnar aerosol properties using sun and star photometry. Rem. Sens. of Clouds and the Atmos. XXI, 10001, 100010K. https://doi.org/10.1117/12.2242372.

Potter, C., Boriah, S., Steinbach, M., Kumar, V., Klooster, S., 2007. Terrestrial vegetation dynamics and global climate controls. Clim. Dynamics, 31(1), 67–78.

Potter, C., Boriah, S., Steinbach, M., Kumar, V., Klooster, S., 2008. Terrestrial vegetation dynamics and global climate controls in North America: 2001–05. Earth Interactions, 12(8), 1–12.

Querol, X., Pey, J., Pandolfi, M., Alastuey, A., Cusack, M., Pérez, N., Moreno, T., Viana, M., Mihalopoulos, N., Kallos, G., Kleanthous, S., 2009. African dust contributions to mean ambient PM10 mass-levels across the Mediterranean Basin. Atmos. Env., 43(28), 4266-4277. https://doi.org/10.1016/j.atmosenv.2009.06.013.

Romano, S., Burlizzi, P., Perrone, M. R., 2016. Experimental determination of short- and long-wave dust radiative effects in the Central Mediterranean and comparison with model results. Atmos. Res., *171*, 5-20. https://doi.org/10.1016/j.atmosres.2015.11.019.

Salvador, P., Alonso-Pérez, S., Pey, J., Artíñano, B., de Bustos, J. J., Alastuey, A., Querol, X., 2014. African dust outbreaks over the western Mediterranean Basin: 11-year characterization of atmospheric circulation patterns and dust source areas. Atmos. Chem. and Phys., 14(13), 6759-6775. https://doi.org/10.5194/acp-14-6759-2014.

Satheesh, S. K., Krishna Moorthy, K., 2005. Radiative effects of natural aerosols: A review. Atmos. Env., *39*(11), 2089-2110. https://doi.org/10.1016/j.atmosenv.2004.12.029.

Satheesh, S. K., Ramanathan, V., 2000. Large differences in tropical aerosol forcing at the top of the atmosphere and Earth's surface. Nature, 405(6782), 60-63. https://doi.org/10.1038/35011039.

S. Segura, S., Estelles, V., Utrillas, M.P., Martínez-Lozano, J.A., 2017. Long term analysis of the columnar and surface aerosol relationship at an urban European coastal site. Atmos. En., 167, 309-322. https://dx.doi.org/10.1016/j.atmosenv.2017.08.012.

Sen, P. K., 1968. Estimates of the regression coefficient based on Kendall's tau. J. of the American statistical association, 63(324), 1379–1389.

Sicard, M., Guerrero-Rascado, J. L., Navas-Guzmán, F., Preißler, J., Molero, F., Toḿs, S., Bravo-Aranda, J. A., Comerón, A., Rocadenbosch, F., Wagner, F., Pujadas, M., Alados-Arboledas, L., 2012. Monitoring of the Eyjafjallajökull volcanic aerosol plume over the Iberian Peninsula by means of four EARLINET lidar stations. Atmos. Chem. and Phys., 12(6), 3115-3130. https://doi.org/10.5194/acp-12-3115-2012.

Sicard, M., Barragan, R., Dulac, F., Alados-Arboledas, L., Mallet, M., 2016. Aerosol optical, microphysical and radiative properties at regional background insular sites in the western Mediterranean. Atmos. Chem. Phys., 16, 12177–12203. https://doi.org/10.5194/acp-16-12177-2016.

https://doi.org/10.1016/j.atmosres.2021.105538

Sivan, C., Manoj, M. G., 2019. Aerosol and cloud radiative forcing over various hot spot regions in India. Advances in Space Res., 64(8), 1577-1591. https://doi.org/10.1016/j.asr.2019.07.028.

Sorribas, M., Andrews, E., Ogren, J. A., del Águila, A., Fraile, R., Sheridan, P., Yela, M. , 2019. Climatological study for understanding the aerosol radiative effects at southwest Atlantic coast of Europe. Atmos. Env., 205, 52-66. https://doi.org/10.1016/j.atmosenv.2019.02.017.

Stocker, T. F., Qin, D., Plattner, G. K., Tignor, M., Allen, S. K., Boschung, J., Nauels, A., Xia, Y., Bex, V., Midgley, P. M., 2013. IPCC, 2013. *Climate Change*.

Titos, G., Del Águila, A., Cazorla, A., Lyamani, H., Casquero-Vera, J. A., Colombi, C., Cuccia, E., Gianelle, V., Močnik, G., Alastuey, A., Olmo, F. J., Alados-Arboledas, L., 2017. Spatial and temporal variability of carbonaceous aerosols: Assessing the impact of biomass burning in the urban environment. The Sci. of the Total Env., *578*, 613-625. https://doi.org/10.1016/j.scitotenv.2016.11.007.

Titos, G., Foyo-Moreno, I., Lyamani, H., Querol, X., Alastuey, A., Alados-Arboledas, L., 2012. Optical properties and chemical composition of aerosol particles at an urban location: An estimation of the aerosol mass scattering and absorption efficiencies. J. of Geophys. Res.: Atmos., 117(D4).

Valenzuela, A., Olmo Reyes, F. J., Lyamani, H., Antón, M., Quirantes Sierra, A., Alados-Arboledas, L., 2012. Aerosol radiative forcing during African desert dust events (2005–2010) over Southeastern Spain. Atmos. Chem. Phys. Discuss., 12, 6593–6622.

https://doi.org/10.1016/j.atmosres.2021.105538

Wu, B.-S., Rufyikiri, A.-S., Orsat, V., Lefsrud, M. G., 2019. Re-interpreting the photosynthetically action radiation (PAR) curve in plants. Plant Science, 289, 110272. https://doi.org/10.1016/j.plantsci.2019.110272.

Xu, J., Bergin, M. H., Greenwald, R., Russell, P. B., 2003. Direct aerosol radiative forcing in the Yangtze delta region of China: Observation and model estimation. J. of Geophys. Res.: Atmos., 108(D2). https://doi.org/10.1029/2002JD002550.

Zhang, M., Wang, Y., Ma, Y., Wang, L., Gong, W., Liu, B., 2018. Spatial distribution and temporal variation of aerosol optical depth and radiative effect in South China and its adjacent area. Atmos. Env., 188, 120-128. https://doi.org/10.1016/j.atmosenv.2018.06.028.

Zhu, Z., Wang, L., Gong, W., Xiong, Y., Hu, B., 2015. Observation and estimation of photosynthetic photon flux density in Southern China. Theor. and App. Clim., 120(3-4), 701-712. https://doi.org/10.1007/s00704-014-1204-1.

Zhuang, B. L., Li, S., Wang, T. J., Deng, J. J., Xie, M., Yin, C. Q., Zhu, J. L., 2013. Direct radiative forcing and climate effects of anthropogenic aerosols with different mixing states over China. Atmos. Env., 79, 349–361.

Zou, L., Lin, A., Wang, L., Xia, X., Gong, W., Zhu, H., Zhao, Z., 2016. Long-term variations of estimated global solar radiation and the influencing factors in Hunan province, China during 1980–2013. Meteorol. and Atmos. Phys., 128(2), 155–165.

https://doi.org/10.1016/j.atmosres.2021.105538